JOURNAL OF COMPUTATIONAL PHYSICS 107, 239–253 (1993)

A Nonreflecting Outlet Boundary Condition for Incompressible Unsteady Navier–Stokes Calculations

G. JIN AND M. BRAZA

Research Group: Transferts en Ecoulements Laminaires et Turbulents, Institut de Mécanique des Fluides de Toulouse, Laboratoire associé au C.N.R.S., URA D0005, Avenue du Professeur Camille Soula, 31400 Toulouse Cedex, France

Received April 10, 1991; revised January 7, 1992

The goal of this work is to adapt a nonreflecting outlet boundary condition, derived from a wave equation, to the numerical solution of the full incompressible Navier–Stokes equations, for an elliptic unsteady free shear flow. The numerical results show that a significant improvement is achieved with this nonreflecting boundary condition, in comparison with the results obtained by using free boundary layer type conditions. The physical phenomena studied concern the onset of the Kelvin–Helmholtz instability in the free (non-forced) shear layer and certain 2D characteristics of transition towards turbulence. These phenomena are simulated naturally, without imposing perturbations. The frequency of the organized vortices and the spread of the mixing layer are correctly predicted. The performances of the method are shown through comparison with the physical experiments. Owing to the nonreflecting boundary conditions, the feedback noises are inhibited effectively, so that the computation domain can be reduced and the dynamic characteristics of the flow are maintained up clearly to the outlet boundary.

1. INTRODUCTION

Artificial boundary conditions are often introduced to the numerical simulations of external flows (e.g., flows around airfoils, jets, mixing layers, wakes past bluff bodies, trailing edge flows, etc.), because there are usually no available data at the free boundaries, which are needed for numerical reasons. Of course, it is hoped that the artificial boundaries and the boundary conditions affect the solutions in such a way that they closely approximate the free space situations which exist in the absence of these boundaries. Hence, especially in the case where the unsteadiness of the flow is intrinsic, special attention has to be made in order to minimize the spurious effects of the artificial boundaries on the solution of the whole field. Concerning the numerical simulation of elliptic external flows, by using the Navier–Stokes equations, Dirichlet type or Neumann type boundary conditions are commonly used. Accordingly, the computation domain must be large enough so that the feedback noise from the boundaries is greatly reduced. Nevertheless, the distance needed is often very long and the cost of the simulation is increased undesirably. Hence, it is necessary to study a kind of boundary conditions needing a reasonable size of the computational domain. In this paper, a nonreflecting type boundary condition is developed for the system of the Navier–Stokes equations in velocity–pressure formulation, applying to an incompressible unsteady free shear flow in the transition towards turbulence. In this kind of flow, complex physical phenomena are related with the onset of intrinsic instabilities, whenever the Reynolds number becomes higher than a critical value. Furthermore, the correct prediction of the onset of such mechanisms as well as of the roll-up process is strongly related with a suitable choice of boundary conditions at infinity.

There have been many substantial works contributing to nonreflecting boundary conditions for dynamical problems of flows. Engquist and Majda [1] [2] developed a nonreflecting boundary condition procedure, in which a pseudo-differential operator was constructed and it was expanded in the deviation of the wave direction from some preferred directions of propagation. In this manner, they designed a boundary condition for absorbing waves incident on the boundary in certain directions. This boundary condition, in first order, was successfully tested by Kwak [3] on the small-disturbance equations for unsteady transonic flows about airfoils. It was demonstrated that the computation domain can be reduced considerably with this nonreflecting boundary approximation procedure. Recently, a comparative study of this type of condition was reported in the work of Blaschak and Kriegsmann [4]. Similar nonreflecting boundary conditions for hyperbolic systems were reported by Hedstrom [5] and Thompson [6]. In the work of Halpern [7] an absorbing boundary condition of this kind is suggested for a linear advection diffusion equation.

Bayliss and Turkel [8, 9] developed a radiation boundary condition approach. By assuming that in the far-field the equations reduce to some simple forms, an asymptotic expansion solution to the model equation is then constructed in terms of a reciprocal radius from the origin. This

0021-9991/93 $5.00

procedure of matching the solution to an expansion that is valid near infinity requires some knowledge of the solution in the neighborhood of infinity. This method was applied, by Bayliss, Gunzburger, and Turkel [10], to elliptic equations such as the Laplace and the Helmholtz equations. In [8, 9] it was used in the computation of the full Navier–Stokes equations for steady compressible flows. It has been shown that this type of boundary condition can accelerate significantly the convergence to steady state.

Rudy and Strikwerda [11] applied the techniques of Engquist and Majda to subsonic Navier–Stokes calculations for obtaining a steady state. By assuming that the pressure is the only physical quantity known at the outlet boundary of the computation domain, they considered a steady-state inviscid solution combined with a perturbation and in this way they constructed a nonreflecting boundary condition which depends on a free parameter. Optimal choice of the parameter can substantially accelerate convergence to the steady state. Nataf [12] designed a nonreflecting boundary condition on the stream function for the steady incompressible Navier–Stokes equations in vorticity-stream function formulation, which was proved to be the most accurate and efficient.

There are few attempts, to our knowledge, to use non-reflecting type boundary conditions for the Navier–Stokes equations concerning an incompressible unsteady elliptic flow. The difficulty comes from the nonlinear and diffusive nature of the dyamics of this kind of flow. The phenomena which will be analysed are related to the transition towards turbulence in a free shear layer flow, at a moderate Reynolds number (Re = 2000). A number of experimental and numerical studies have shown that an intrinsic unsteadiness occurs in the flow, due to the onset of a Kelvin–Helmholtz instability [13, 14]. This unsteadiness, followed by the establishment of the rolled-up process and the appearance of vortices after a transition region, depends on the velocity gradient and Reynolds number. The theoretical model adopted here for the prediction of this kind of flow is the system of the Navier–Stokes equations, because this model allows us to take into account non-linear effects related with the above phenomena. A previous study of such phenomena has been done by Kourta, Braza, Chassaing, and Ha Minh [14], using free boundary layer type conditions. In the present paper, we study an outlet boundary condition to satisfy following exigencies:

— Non-reflecting properties on the outlet boundary;

— Respect of non-linear and diffusive mechanisms of the flow;

— Matching with the Navier–Stokes systems adopted inside the domain.

In Section 2, the governing equations and numerical method are presented. The boundary conditions are discussed in Section 3. Section 4 contains the numerical results to show the performances of the present boundary conditions, in comparison with the experiments. Finally, the conclusions are given in Section 5.

2. GOVERNING EQUATIONS AND NUMERICAL METHOD

The theoretical equations are those of isothermal and incompressible viscous flow. They are written in a cartesian coordinates system, in conservative form, and with respect to the dimensionless variables,

$$\mathbf{V}^* = \frac{\mathbf{V}}{U_0}, \qquad x^* = \frac{x}{L_0}, \qquad y^* = \frac{y}{L_0}, \qquad t^* = \frac{t}{T_0}, \qquad P^* = \frac{P}{P_0}, \tag{2.1}$$

obtained by the following reference variables:

$$U_0, \quad L_0, \quad \rho_0, \quad T_0 = \frac{L_0}{U_0}, \quad P_0 = \frac{1}{2}\rho U_0^2. \tag{2.2}$$

In the following, the symbol (*) is suppressed for the dimensionless variables.

For a two-dimensional flow, the equations of motion are written

$$\frac{\partial u}{\partial x} + \frac{\partial v}{\partial y} = 0 \tag{2.3}$$

$$\frac{\partial u}{\partial t} + \operatorname{div}(u\mathbf{V}) - \frac{1}{\mathrm{Re}} \operatorname{div}(\mathbf{grad}\, u) = -\frac{\partial P}{\partial x} \tag{2.4}$$

$$\frac{\partial v}{\partial t} + \operatorname{div}(v\mathbf{V}) - \frac{1}{\mathrm{Re}} \operatorname{div}(\mathbf{grad}\, v) = -\frac{\partial P}{\partial y}, \tag{2.5}$$

where

$$\mathrm{Re} = \frac{U_0 L_0 \rho_0}{\mu}$$

is the Reynolds number and μ is the molecular viscosity.

The numerical method is developed by Braza and registered as solver DIANE (directions implicites alternées pour Navier–Stokes equations), in the CNUSC-IBM joint project C3NI (Centre de Compétences en Calcul Numérique Intensif) [15–17].

The momentum equations are solved at the $(n+1)$ time

step for an approximate velocity field $\mathbf{V}^*$ by using a guessed pressure field, $P^* = P^n$:

$$\frac{u^* - u^n}{\Delta t} + \operatorname{div}(u^*\mathbf{V}^n) - \frac{1}{\mathrm{Re}}\operatorname{div}(\mathbf{grad}\, u^*) = -\frac{\partial P^n}{\partial x}$$
$$\frac{v^* - v^n}{\Delta t} + \operatorname{div}(v^*\mathbf{V}^n) - \frac{1}{\mathrm{Re}}\operatorname{div}(\mathbf{grad}\, v^*) = -\frac{\partial P^n}{\partial y}. \tag{2.6}$$

The true velocity field at the $(n+1)$ time step is given by

$$\mathbf{V}^{n+1} = \mathbf{V}^* - \mathbf{grad}\, \phi, \tag{2.7}$$

where ϕ is an auxiliary potential function. This is calculated by the Poisson equation

$$\nabla^2\phi = \operatorname{div}(\mathbf{V}^*), \tag{2.8}$$

obtained by claiming:

$$\operatorname{div}(\mathbf{V}^{n+1}) = 0. \tag{2.9}$$

The pressure at the $(n+1)$ time step is calculated by the equation

$$\mathbf{grad}\, P^{n+1} = \mathbf{grad}\left(P^n + \frac{\phi}{\Delta t}\right) + \operatorname{div}(\mathbf{V}^n\, \mathbf{grad}\, \phi)$$
$$-\frac{1}{\mathrm{Re}}\nabla^2(\mathbf{grad}\, \phi), \tag{2.10}$$

or by the more simplified equation,

$$P^{n+1} = P^n + \phi/\Delta t, \tag{2.11}$$

giving practically the same results for a moderate Reynolds number range [16, 17].

A semi-implicit second-order accurate scheme in time and space is used. The equations are integrated over finite volumes. The staggered grids of Harlow and Welch [18] are used for velocity and pressure fields. An alternating direction implicit method is used for the time-dependent discretization. The detailed descriptions can be found in [15–17].

3. BOUNDARY CONDITIONS

The domain of computations is shown in Fig. 1. At the entry of the domain, the boundary conditions are Dirichlet type, imposed by the nature of the velocity gradient (Fig. 1):

$$u(0, y) = \begin{cases} 0.5, & 0 < y < h, \\ 1.0, & h < y < H, \end{cases}$$
$$v(0, y) = 0. \tag{3.1}$$

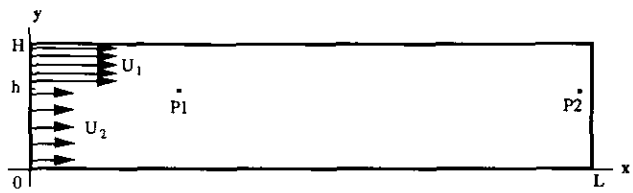

FIG. 1. Computation domain.

On the upper and lower free boundaries, different kinds of boundary conditions were tested by Kourta *et al.* [14]. It was found that the more appropriate conditions were those derived by considering these boundaries as streamlines, where

$$v = 0, \qquad \frac{\partial u}{\partial y} = 0. \tag{3.2}$$

Outlet Boundary Conditions of Type I

The outlet boundary condition plays an important role in the numerical simulations of free flows. It is usually supposed that this boundary is put sufficiently far from the origin of the mixing layer, so that the classical free boundary layer hypotheses and the similarity lows are satisfied. Hence the following boundary conditions are used, which are derived by supposing that the flow has a prefered direction (along x) and $\partial\mathbf{V}/\partial t = 0$ at the boundary:

$$\frac{\partial^2 u}{\partial x^2} = 0, \qquad \frac{\partial v}{\partial x} = 0. \tag{3.3}$$

These boundary conditions were successfully used for the flow past a backward facing step [19] and for a mixing layer flow [14] at lower Reynolds numbers.

However, this type of boundary conditions requires a large distance x. This leads to heavy CPU time and memory storage. If the computation domain is not large enough so that the flow could reach the region of the similarity assumptions, the above outlet boundary conditions always present the problem of non-physical feedbacks. As will be shown in Section 4, although the instability nature and roll-up processes of the flow have been simulated well, it appears that the vortices hit against a "wall," while they are going out of the domain.

The computations are carried out with this kind of boundary condition in order to examine the efficiency of the nonreflecting boundary conditions, derived in the following.

Nonreflecting Outlet Boundary Conditions (Type II)

Since orderly coherent structures and sequential merging of vortices constitute the primary mechanisms for the spreading of the mixing layer in the downstream direction, and because the flow shows a pseudo-periodicity in time

and in space [13, 20, 21], the velocity field displays qualitatively wavelike features. Hence, the boundary conditions should simulate the propagation of waves out of the computational domain; that is to say, they should allow the motion of outgoing flow to pass through the boundary without being reflected. In this way, we consider using a wave equation to match the Navier–Stokes equations on the outlet boundary for the present viscous unsteady problem.

The velocity vector $\mathbf{V}$ is considered as a transported wave quantity incident on the boundary. Considering the feature of the present viscous elliptic flow, an anisotropic propagation wave equation is taken on the boundary. In two dimensions, it can be written as

$$\frac{\partial^2 \mathbf{V}}{\partial t^2} - c_x^2 \frac{\partial^2 \mathbf{V}}{\partial x^2} - c_y^2 \frac{\partial^2 \mathbf{V}}{\partial y^2} = 0; \tag{3.4a}$$

c_x and c_y are the characteristic velocities of the wave propagation in the x and y directions, respectively. The technique of Engquist and Majda [1, 2, 4] is adopted to provide the absorption properties, and the pseudo-differential operators

$$L\mathbf{V} \equiv c_x^2 D_x^2 \mathbf{V} + c_y^2 D_y^2 \mathbf{V} - D_t^2 \mathbf{V} = 0 \tag{3.4b}$$

are introduced, where D_x^2, D_y^2, and D_t^2 designate the second partial derivatives in respect to the x, y directions and to the time t. The factorization of the wave operator, L, gives

$$L\mathbf{V} = L^+ L^- \mathbf{V} = 0,$$

where

$$L^+ \equiv c_x D_x + D_t \sqrt{1 - s^2} \tag{3.5a}$$

and

$$L^- \equiv c_x D_x - D_t \sqrt{1 - s^2} \tag{3.5b}$$

with:

$$s = c_y D_y / D_t. \tag{3.6}$$

The relation

$$L^+ \mathbf{V} = 0 \tag{3.7}$$

applied to the outlet boundary is a total absorption (non-reflecting) condition [1, 2, 4].

As the pseudo-differential operator is nonlocal in both time and space variables, the following Padé-approximations of the square root $\sqrt{1 - s^2}$ are used:

First approximation,

$$\sqrt{1 - s^2} \approx 1; \tag{3.8}$$

then (3.7) can be written

$$(c_x D_x + D_t)\mathbf{V} = 0. \tag{3.9}$$

Second approximation,

$$\sqrt{1 - s^2} \approx 1 - \tfrac{1}{2} s^2; \tag{3.10}$$

then (3.7) can be written as

$$\left(c_x D_x + D_t - \frac{c_y^2}{2D_t} D_y^2\right)\mathbf{V} = 0. \tag{3.11}$$

The coefficient c_y appears because of the anisotropic character in present analysis.

In comparison with the Navier–Stokes equations, the diffusion term, in (3.11), is reasonably set as $\nu \partial^2 \mathbf{V}/\partial y^2$ and the propagation velocity c_x is made equal to u component in order to match this equation to the Navier–Stokes ones. Hence, the equation

$$\frac{\partial \mathbf{V}}{\partial t} + u \frac{\partial \mathbf{V}}{\partial x} - \nu \frac{\partial^2 \mathbf{V}}{\partial y^2} = 0 \tag{3.12}$$

is obtained, where ν is the coefficient of kinematic viscosity.

It can be noted that Eq. (3.12) maintains a non-linear character as the Navier–Stokes equations do at the inner of domain and it ensures a non-reflecting type condition. This equation is then used as an outlet boundary condition in the present Navier–Stokes solver.

An implicit second-order central approximation in time is used for the discretisation of Eq. (3.12) [22]. We have

$$\frac{\mathbf{V}^{n+1/2} - \mathbf{V}^n}{\Delta t/2} + \frac{u^n}{2}\left[\left(\frac{\partial \mathbf{V}}{\partial x}\right)^{n+1/2} + \left(\frac{\partial \mathbf{V}}{\partial x}\right)^n\right] = \nu \left(\frac{\partial^2 \mathbf{V}}{\partial y^2}\right)^n + O(\Delta t^2) \tag{3.13}$$

for the time step $n + 1/2$ and

$$\frac{\mathbf{V}^{n+1} - \mathbf{V}^n}{\Delta t} + \frac{u^n}{2}\left[\left(\frac{\partial \mathbf{V}}{\partial x}\right)^{n+1} + \left(\frac{\partial \mathbf{V}}{\partial x}\right)^n\right] = \nu \left(\frac{\partial^2 \mathbf{V}}{\partial y^2}\right)^n + O(\Delta t^2) \tag{3.14}$$

for the time step n.

Boundary Conditions for the Function ϕ

The boundary conditions for the auxiliary potential function ϕ are deduced from the velocity conditions and from Eq. (2.7),

$$\mathbf{V}^{n+1} - \mathbf{V}^* = -\mathbf{grad}\ \phi \tag{3.15}$$

by supposing that the velocity vectors $\mathbf{V}^{n+1}$ and $\mathbf{V}^*$ have the same expressions as the boundary conditions.

Hence, at the entry of the domain,

$$\frac{\partial \phi}{\partial x} = 0. \tag{3.16}$$

Along the upper and lower free boundaries,

$$\frac{\partial \phi}{\partial y} = 0. \tag{3.17}$$

At the outlet boundary,

$$\frac{\partial^3 \phi}{\partial x^3} = 0 \tag{3.18}$$

for type I boundary conditions.

For the case of boundary conditions of type II, replacing $\mathbf{V}^{n+1}$ by u^{n+1} and u^*, respectively, in (3.14), we have

$$\frac{u^{n+1} - u^n}{\Delta t} + \frac{u^n}{2}\left[\left(\frac{\partial u}{\partial x}\right)^{n+1} + \left(\frac{\partial u}{\partial x}\right)^n\right] = \nu\left(\frac{\partial^2 u}{\partial y^2}\right)^n + O(\Delta t^2) \tag{3.19}$$

and

$$\frac{u^* - u^n}{\Delta t} + \frac{u^n}{2}\left[\left(\frac{\partial u}{\partial x}\right)^* + \left(\frac{\partial u}{\partial x}\right)^n\right] = \nu\left(\frac{\partial^2 u}{\partial y^2}\right)^n + O(\Delta t^2); \tag{3.20}$$

substracting (3.20) from (3.19), we can obtain

$$\frac{1}{\Delta t}(u^{n+1} - u^*) + \frac{u^n}{2}\frac{\partial}{\partial x}(u^{n+1} - u^*) = 0. \tag{3.21}$$

By claiming (2.7)

$$u^{n+1} - u^* = -\partial\phi/\partial x, \tag{3.22}$$

we obtain the outlet boundary condition for ϕ:

$$\frac{\partial \phi}{\partial x} + \frac{u^n \Delta t}{2}\frac{\partial^2 \phi}{\partial x^2} = 0. \tag{3.23}$$

The initial conditions are taken to be those of the ideal fluid flow, with respect to the inlet velocity gradient in the whole region (Fig. 1). In [14], it was demonstrated that the flow forgets the initial conditions after a transient phase.

4. RESULTS

Three numerical tests are carried out on the IBM 3090-600-VF computer of the CNUSC (Centre National Universitaire Sud de Calcul). The computation domain is shown in Fig. 1 and the numerical parameters are given on Table I. The Reynolds number 2000 is based on a unity length and velocity scale. In the following, the performances of the outlet boundary conditions of type I and type II are compared first. Then the influence of the size of the domain (x direction), with the boundary condition of type II, is analysed. Comparisons with experimental results are finally given.

With both boundary conditions (tests A and B), the solver is able to generate naturally, without imposing perturbations, the onset of a non-linear instability, leading to transition waves followed by the roll-up process. These features, analysed experimentally in the work of Brown and

TABLE I

Numerical Parameters

Test of computation	Number of grid points ($NX * NY$)	Size of domain ($L * H$)	h	$\Delta x_{\min}$ / $\Delta y_{\min}$	Δt	Type of boundary condition	CPU time/ time-step (second)	Total time step
A	102 × 36	67.19 × 14.69	10.30	0.1	0.01	I	0.568	15,000
B	102 × 36	67.19 × 14.69	10.30	0.1	0.01	II	0.574	15,000
C	92 × 36	59.15 × 14.69	10.30	0.1	0.01	II	0.465	9,000

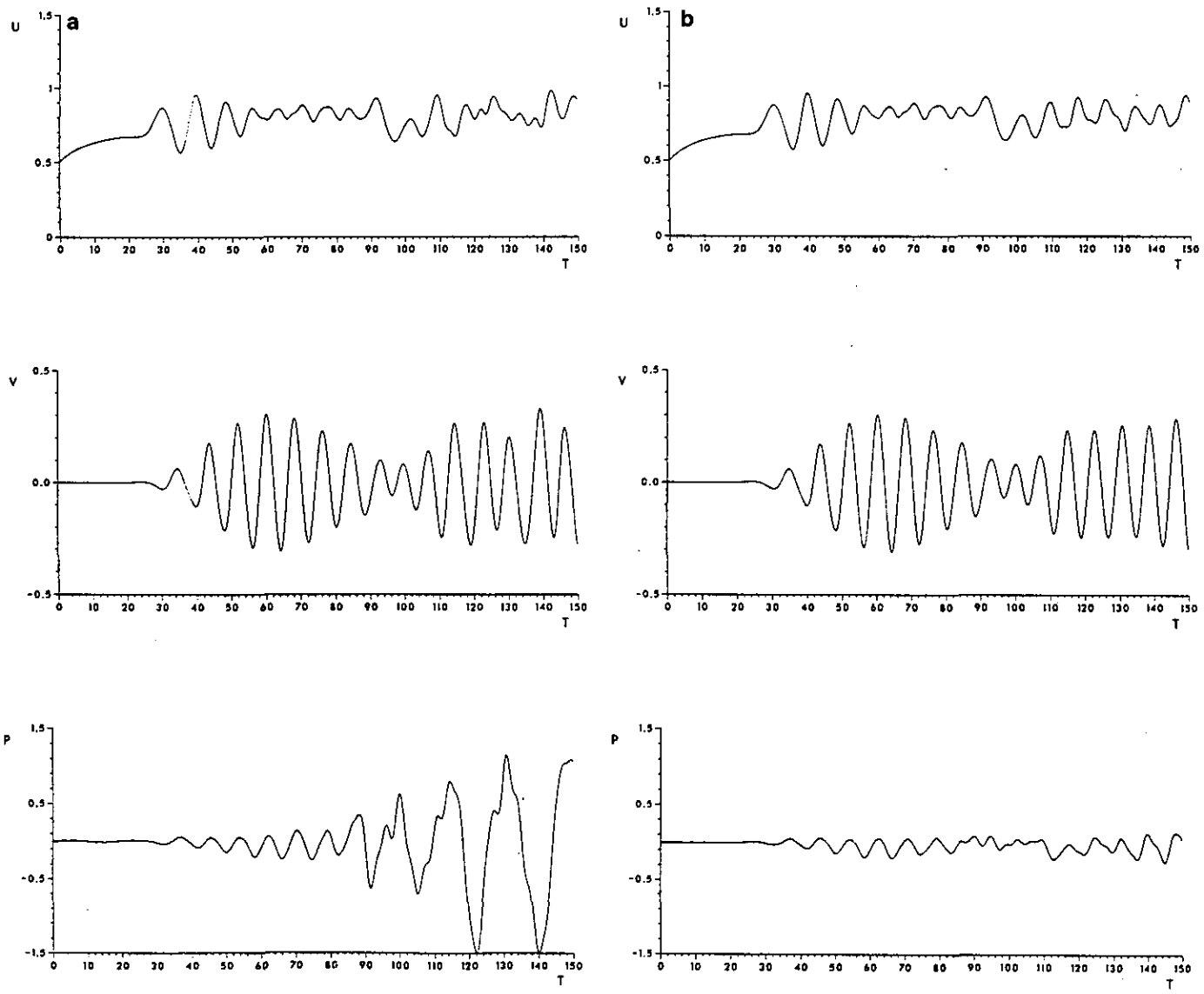

FIG. 2. Time-dependent evolution of the velocity and the pressure coefficient, $x = 18.31$, $y = 10.25$: (a) with boundary conditions of type I; (b) with nonreflecting boundary conditions.

Roshko [13], Freymuth [20], Ho and Huerre [21], among others, are a consequence of the steep velocity gradient at the origin of a free shear layer, whenever the Reynolds number becomes higher than a critical value. In [14], these mechanisms were simulated numerically for lower Reynolds number values. In the present case (Re = 2000), the same mechanisms are obtained.

Figure 2 shows the time-dependent evolutions of the velocity and pressure coefficients at $x = 18.31$, $y = 10.25$ (point P1 in Fig. 1), with the boundary conditions of type I and type II, respectively. It is recalled that the pressure coefficient is calculated as $(P - P_0)/0.5\rho U_1^2$. The periodic character of the flow is shown clearly. Nevertheless, the boundary conditions of type I seem to display some nonphysical irregularities when $t > 95$ (Fig. 2a). Especially, the pressure coefficient oscillations increase dramatically. This problem becomes more severe downstream (see Fig. 3a, $x = 65.77$, $y = 10.25$, point P2 in Fig. 1). It seems that the flow is alternatively pressed and drawn by the outlet boundary before and after the vortices traverse across the boundary. However, these irregularities are greatly inhibited in the case of boundary conditions II.

Figure 4 shows the iso-pressure coefficient plot with boundary conditions I, at $t = 60$. An irregular behaviour can be seen near the outlet boundary. This problem becomes more pronounced at $t = 100$ (Fig. 5), where the structure of

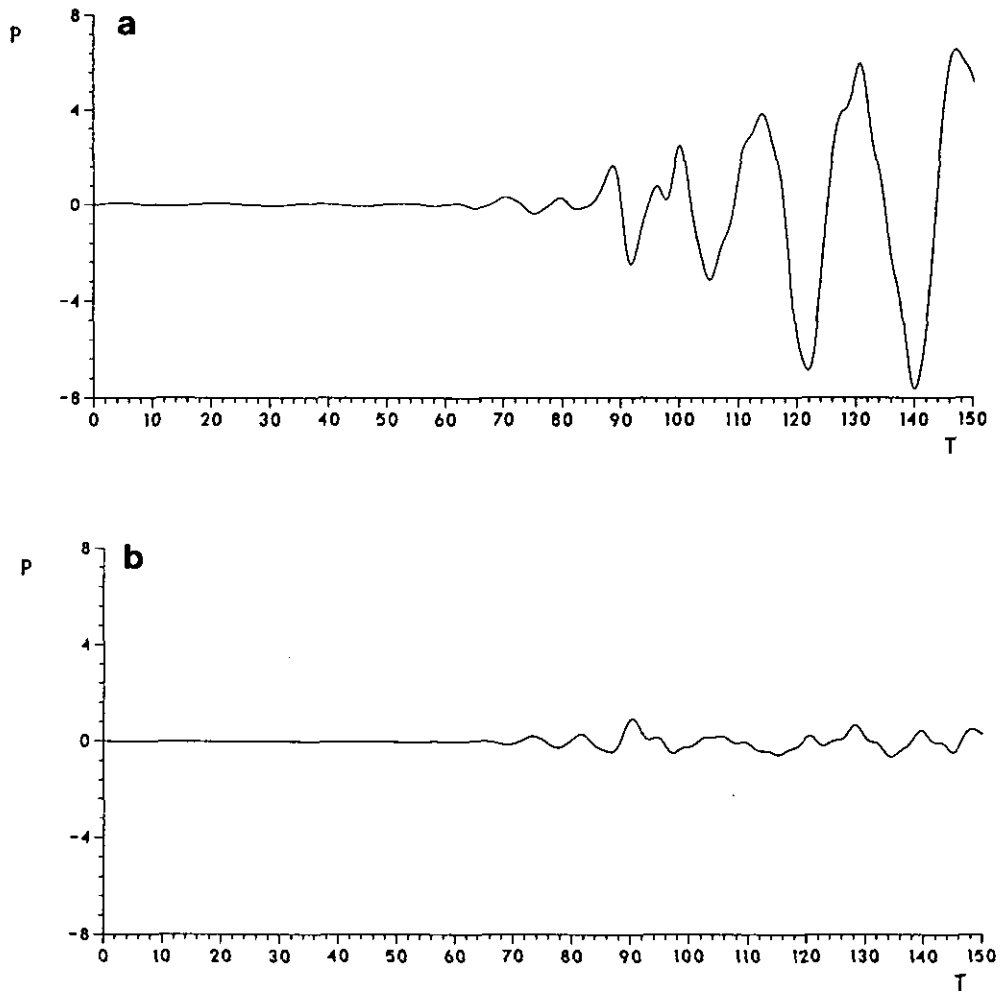

FIG. 3. Time-dependent evolution of the pressure coefficient, $x = 65.77$, $y = 10.25$: (a) with boundary conditions I; (b) with boundary conditions II.

the eddies has almost disappeared in the vicinity of the outlet boundary and a non-physical pressure gradient has developed.

On the contrary, such irregular phenomena are not observed in the case of the nonreflecting boundary conditions. Figure 6 shows the isobars at $t = 60$. It is remarkable that the vortices are generated naturally and that no irregular developments occur. Moreover, there are a series of small vortices appearing downstream, which are completely damped in the case of boundary condition I. At $t = 100$, Fig. 7 shows a correct development of the organized structures, travelling through the numerical boundary without blockage effects. It is noticeable that the organized eddies have a repetitive character in time and space, which is a main property of a coherent flow pattern.

Another insight of the history of the flow, including the onset of instability, the waviness of the shear layer, and finally the development of organized coherent structures can be obtained by the help of streaklines. Figures 8 and 9 show the velocity fields and the streaklines, when the first vortex reaches the outlet boundary, with boundary conditions I and II, respectively. The features of the roll-up process are shown clearly, in agreement with the experimental visualizations [13, 20, 21]. Figures 10 and 11 are the zooms of Figs. 8 and 9, respectively, for the outlet region. In Figure 10, the v component values of the velocity field are excessively high and directed towards the lower boundary, as if the flow is against a "wall." Nevertheless, with the nonreflecting boundary conditions (Fig. 11), the velocity field keeps up a physically correct aspect in this region.

The performances of both boundary conditions are also shown through the accuracy of solving the mass conservation equation. In the present method, this corresponds to the convergence errors of the Poisson equation, solved by an iterative ADI method [15, 16]. The convergence is achieved after 20 iterations at each time step. The maximum convergence errors over all the domain are plotted as a function of time in Fig. 12. The errors for type I are of an

FIG. 4. Isobars with boundary conditions of type I, Re = 2000, $t = 60$.

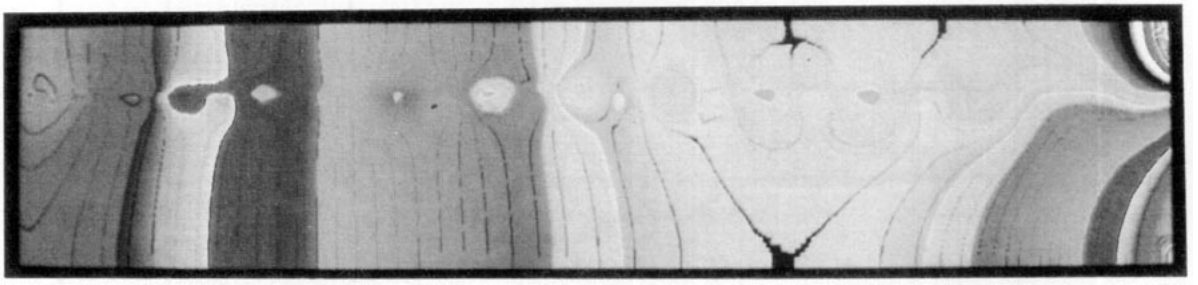

FIG. 5. Same as Fig. 4, $t = 100$.

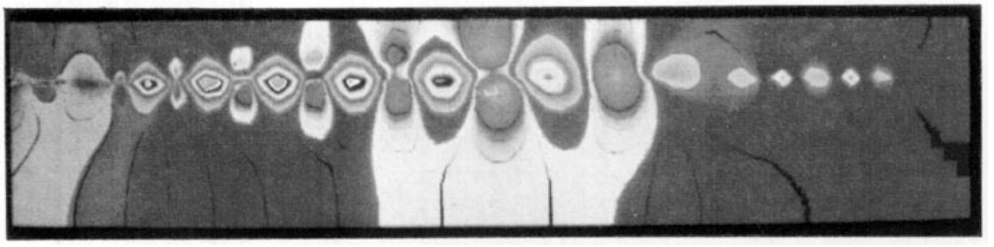

FIG. 6. Isobars with nonreflecting boundary conditions, $t = 60$.

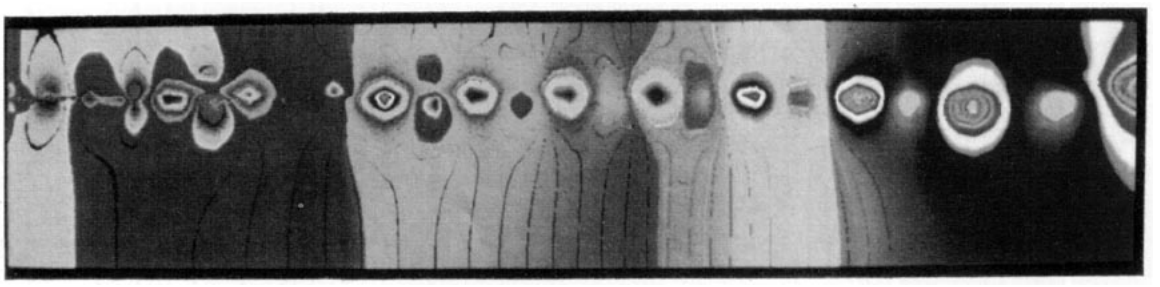

FIG. 7. Same as Fig. 6, $t = 100$.

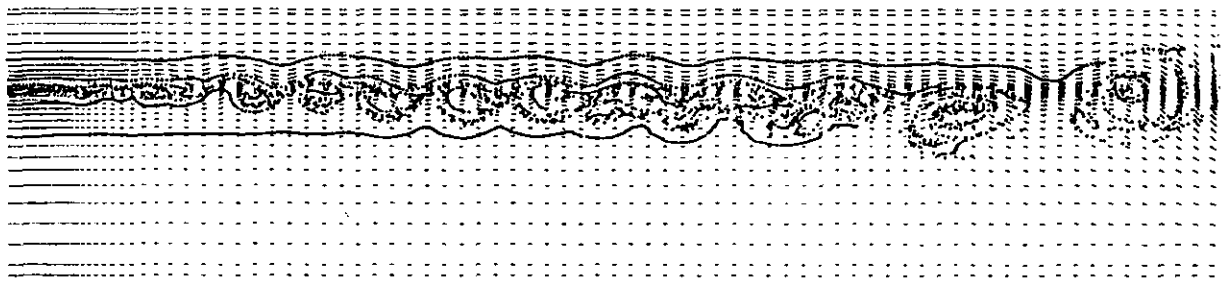

FIG. 8. Velocity field and streaklines, $t = 95$, boundary conditions I.

order 10^{-4} and have an increasing tendency, whereas for type II, they are of an order 10^{-5} only and show a more stable evolution in time. The above results show clearly the superiority of the nonreflecting boundary conditions over those of type I.

The influence of the computation domain size is now examined. The computations are carried out with a smaller value of L ($L = 59.15$, test C, see Table I) to compare with the preceding case (test B, $L = 67.19$). Figures 13a and 13b show the velocity fields and the streaklines at $t = 87$ for the two cases. It can be seen that there is almost no difference in both results. For the same instant, Fig. 14 shows the isobars of the two cases within the smaller domain area. A good agreement for B and C is shown. This proves the efficiency of the nonreflecting type boundary conditions, which allow us to work with a reduced length of computation domain.

The temporal mean velocity profiles, with the nonreflecting boundary conditions (test B), at several x positions are given in Fig. 15 for a u component. Through these figures, the growth of the mixing layer is clearly pointed out. A reliable measure of the spread of the free mixing layer is the integral momentum thickness [23] defined as

$$\theta(x) = \frac{1}{(U_1 - U_2)^2} \int_{-\infty}^{\infty} [U_1 - \bar{u}(x, y)][\bar{u}(x, y) - U_2]\, dy; \tag{4.1}$$

θ is determined by integration of the mean velocity profiles shown in Fig. 15. The results are plotted in Fig. 16a. In the region $x < 13$, the mixing layer has a parabolic spread due to laminar growth and reaches a linear growth for $x > 13$, due to the roll-up process and to the vortex mergings. This is in accordance with the physical experiments [24] (Fig. 16b).

The spectra of streamwise velocity fluctuation at several points are shown in Fig. 17. This is obtained by taking a fast Fourier transform of the time-dependent evolution of the velocity. The spectral resolution is 0.012, obtained by using 8192 (2^{13}) time-domain points. A frequency peak appears systematically in the spectra, which corresponds to the fundamental frequency f_m, the shedding frequency of Kelvin–Helmholtz vortices. Other peaks appear at $2f_m$, $3f_m$, ... The corresponding Strouhal number is found to be

$$St_m = \frac{f_m \theta_0}{U_1} = 0.122 \tag{4.2}$$

with $\theta_0 = 0.025$, the initial momentum thickness. Accordingly, f_m is equal to $4.88 H_z$. This is quite close to the experiment result $5.06 H_z$ [24].

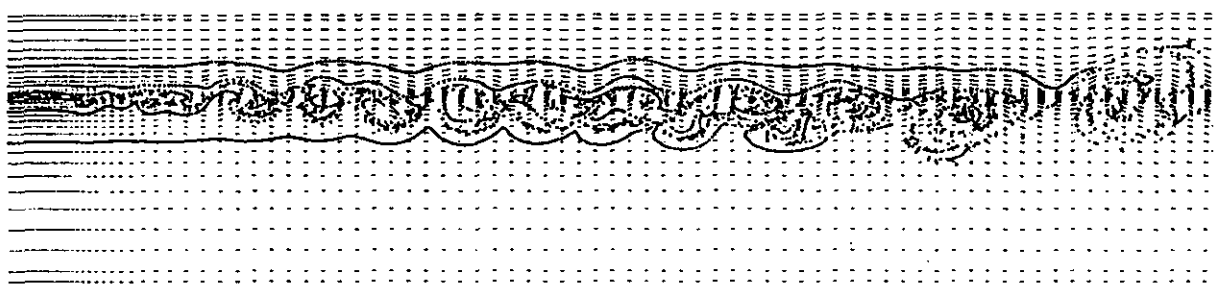

FIG. 9. Velocity field and streaklines, $t = 95$, boundary conditions II.

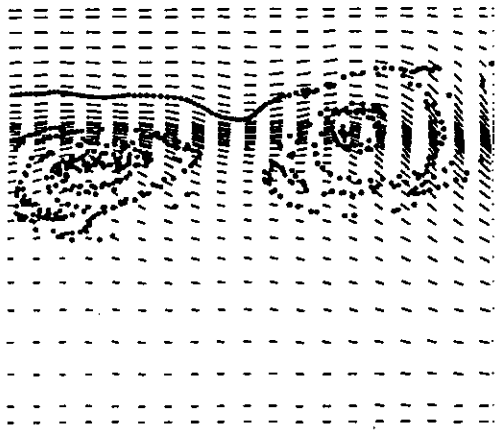

FIG. 10. Zoom of Fig. 10, outlet region, boundary conditions I.

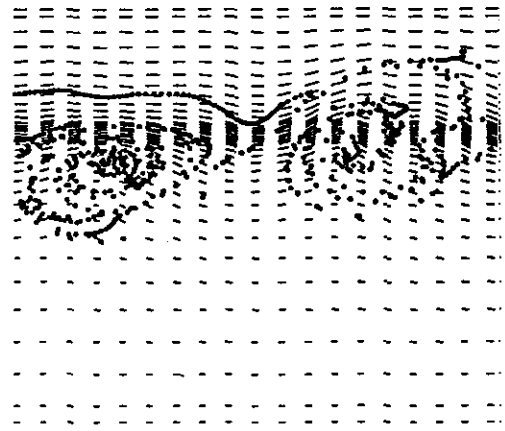

FIG. 11. Zoom of Fig. 11, outlet region, boundary conditions II.

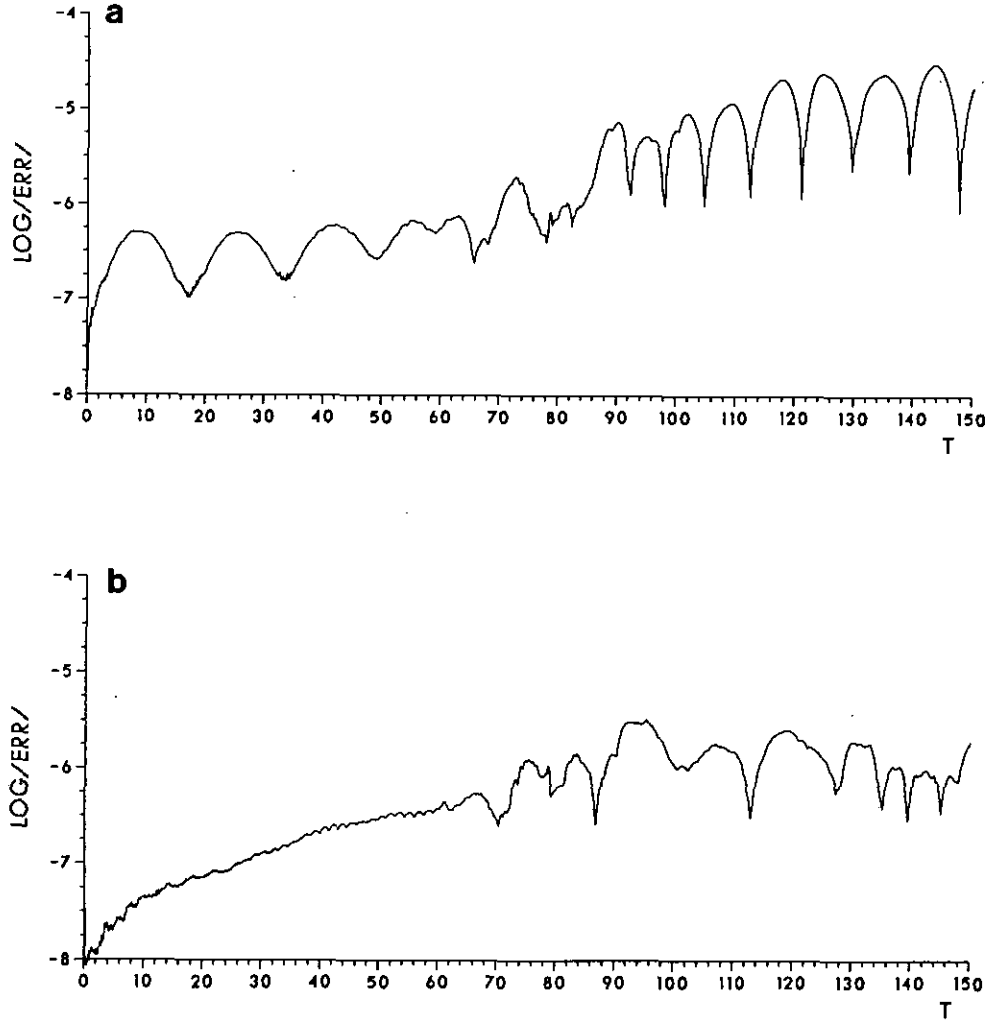

FIG. 12. Evolution of convergence error for Poisson equation: (a) with boundary conditions I; (b) with boundary conditions II.

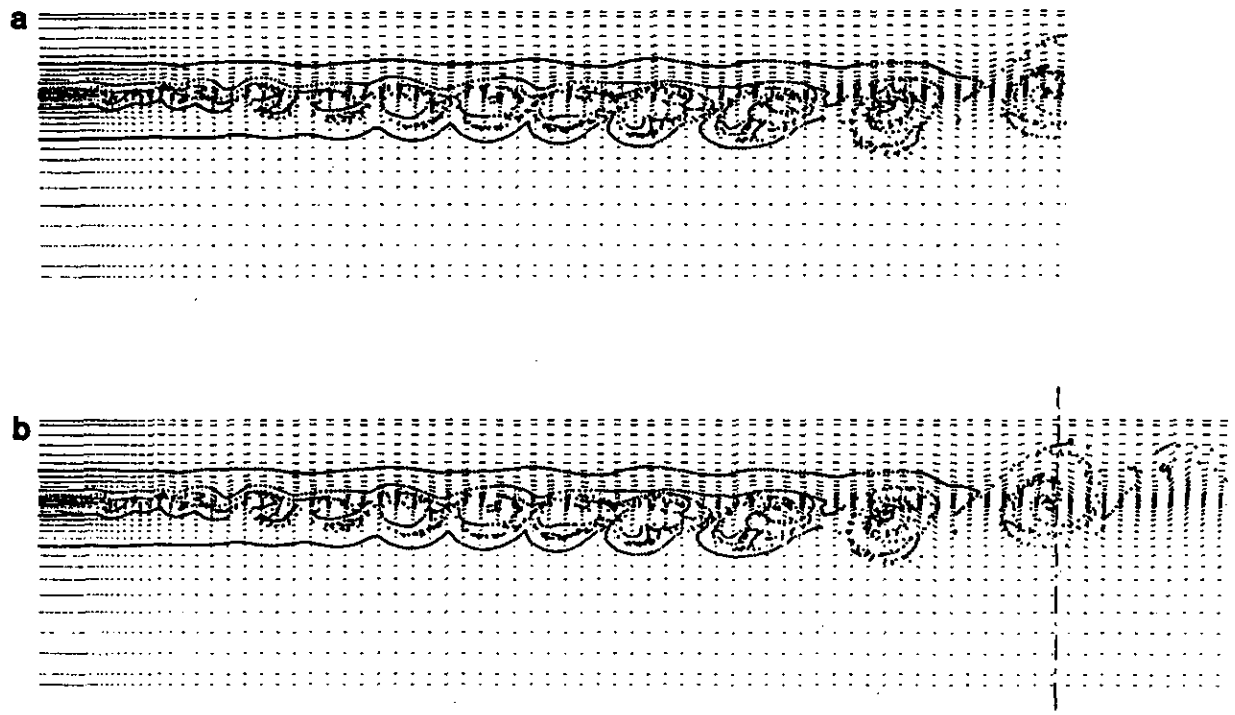

FIG. 13. Velocity field and streaklines, $t = 87$: (a) test C; (b) test B.

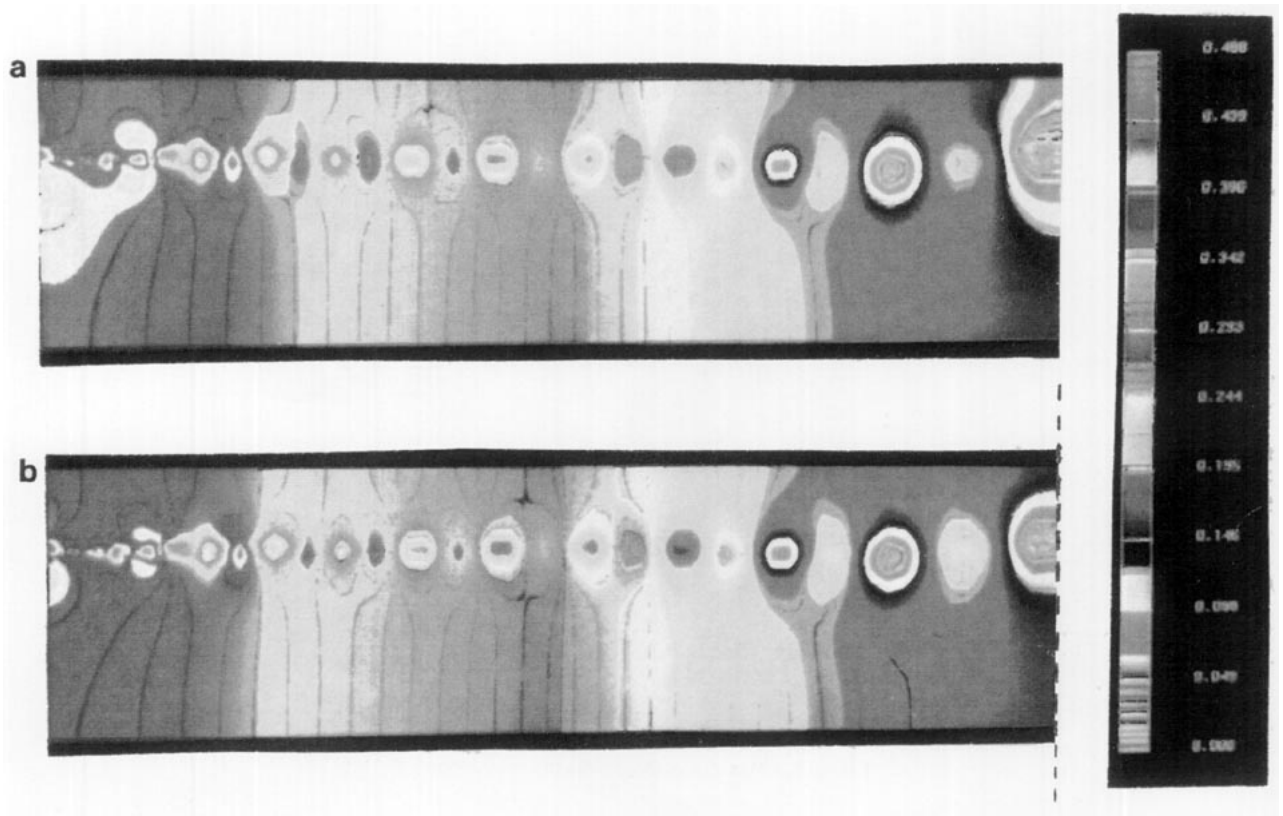

FIG. 14. Isobars at $t = 87$: (a) test C; (b) test B.

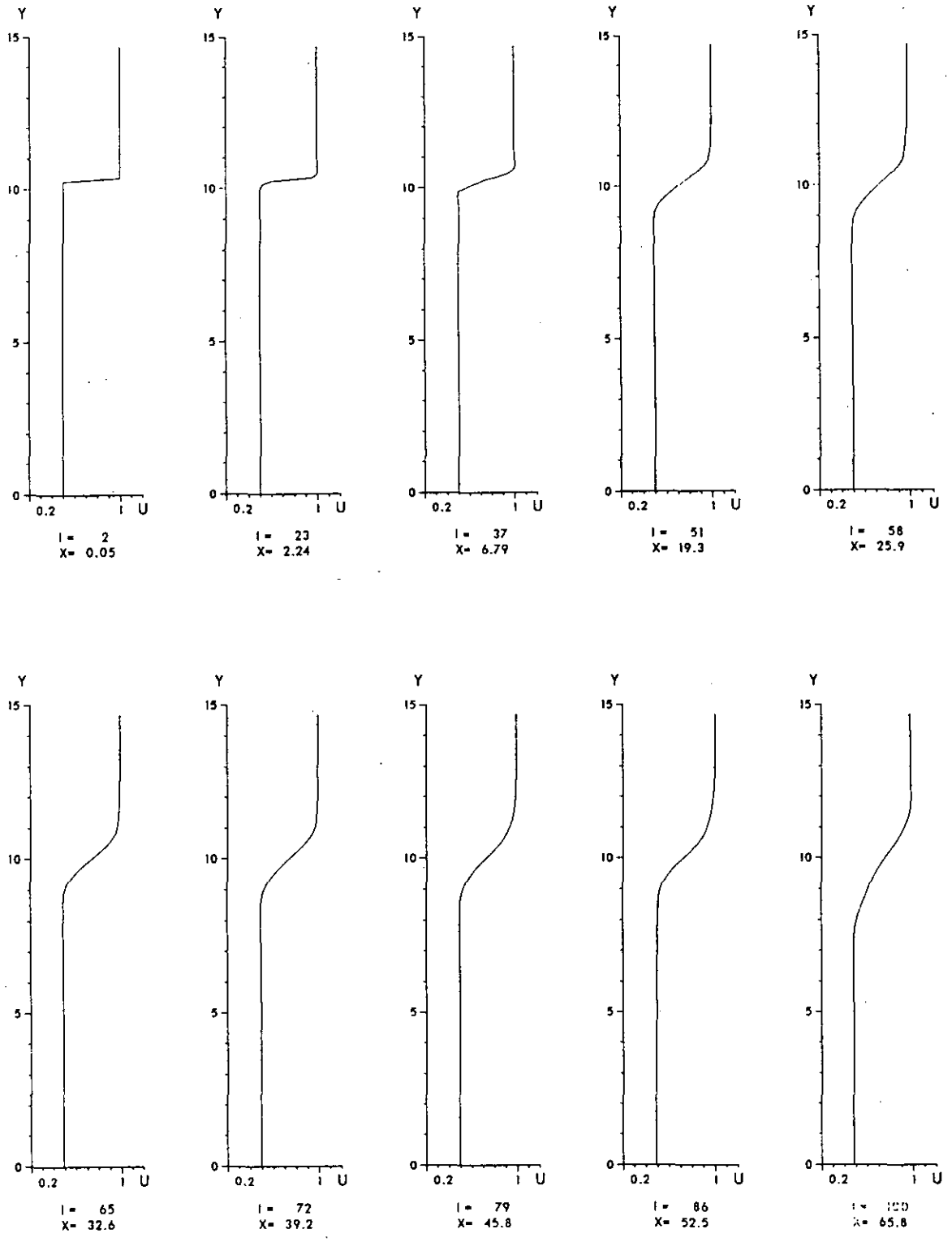

FIG. 15. Mean velocity profiles of u component.

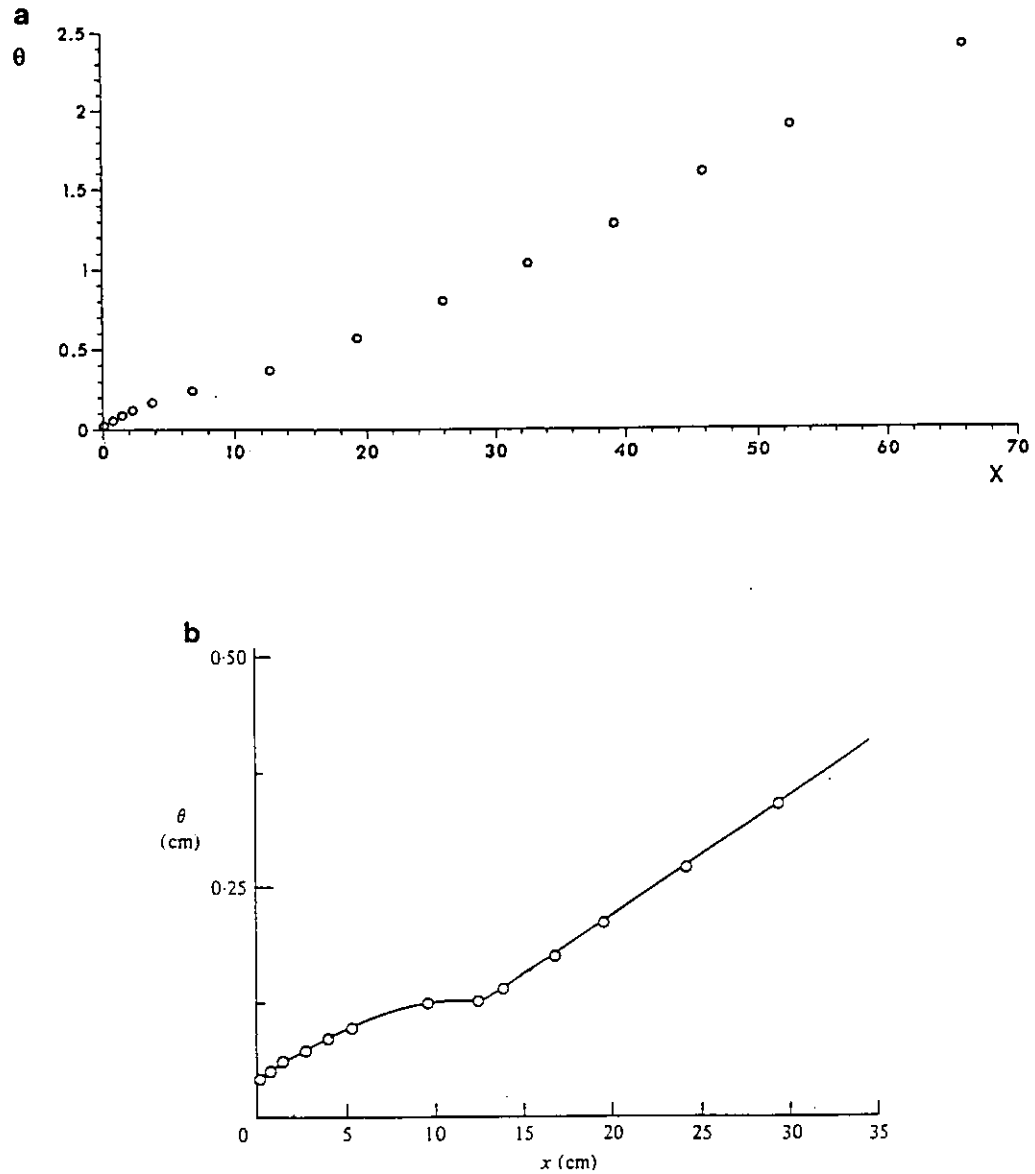

FIG. 16. (a) Spread of the mixing layer. (b) Spread of an unforced mixing layer, experimental results by Ho and Huang [24]; θ is the momentum thickness on the high-speed side.

5. CONCLUSION

A nonreflecting boundary condition is studied, which can be correctly matched with the Navier–Stokes equations, governing an incompressible unsteady free shear layer flow. The numerical simulation, associated with this boundary condition, is able to predict naturally, without imposing perturbations, the onset of instability and the development of organized structures in the free shear layer, concerning the transition of this flow towards turbulence. The numerical results have shown a noticeable efficiency of the nonreflecting boundary condition which minimizes considerably the feedback noises and allows us to reduce the length of computation domain. Moreover, the dynamical characteristics of the flow, such as the roll-up process, the growth of mixing layer, and the predominant frequency, are predicted correctly in agreement with the experiments. It can also be noted that this boundary condition has the advantage of being easily implemented for other types of incompressible unsteady elliptic flows, e.g., jets, flows around aerofoils, and bluff bodies.

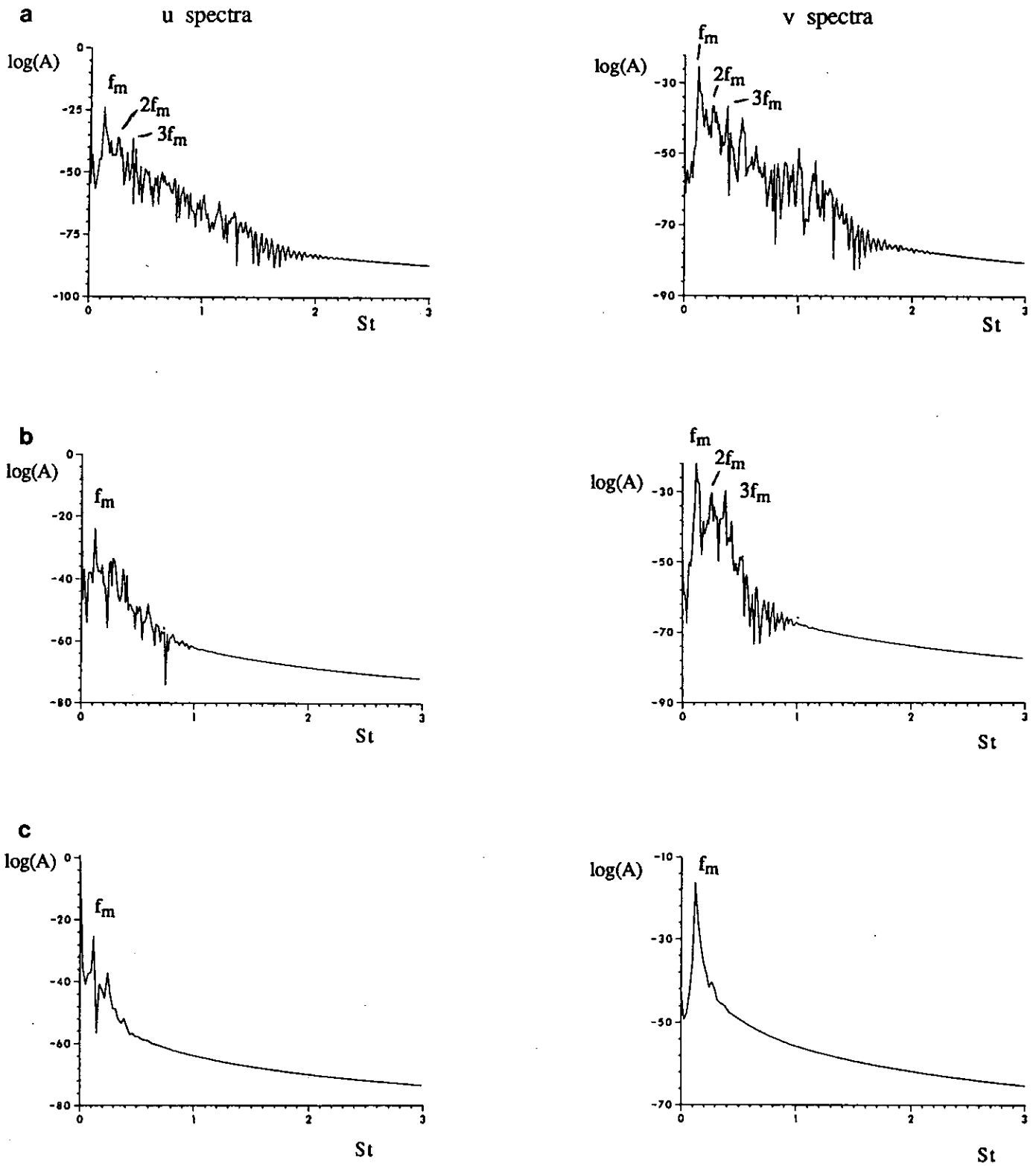

FIG. 17. Spectra of the time-dependent velocity components: (a) $x = 0.65$; (b) $x = 3.75$; (c) $x = 18.31$.

ACKNOWLEDGMENTS

The authors thank the staff of the CNUSC and C3NI for their precious aid to optimize the solver DIANE and for the CPU time supplied on the IBM 3090-600-VF computer of the CNUSC to carry out the present simulation. They are also grateful to Professors P. Chassaing and H. Ha Minh and to Dr. A. Kourta, Dr. H. Boisson, and Dr. A. Sevrain, for their fruitful discussions. The graphics software for the isobars has been developed on the Silicon Graphics station of the research group TELET (Transferts en Ecoulements Laminaires et Turbulents), in the Institut de Mécanique des Fluides de Toulouse, by D. Astruc, H. C. Boisson, L. Bombaud, J. L. Estivalezes, and G. Leblanc. The authors thank also Mr. M. Brunato for the colour picture presentation, Mrs. J. Rambouil for the reprographics, and Mr. J. Bonnefont, Mr. J. C. Pons, Mrs. M. C. Tristani, Mrs. C. Domene for their technical assistance.

REFERENCES

1. B. Engquist and A. Majda, *Math. Comput.* **31**, 629 (1977).
2. B. Engquist and A. Majda, *J. Comput. Phys.* **40**, 91 (1981).
3. D. Kwak, *AIAA J.* **19**, 1401 (1981).
4. J. G. Blaschak and G. A. Kriegsmann, *J. Comput. Phys.* **77**, 109 (1988).
5. G. W. Hedstrom, *J. Comput. Phys.* **30**, 222 (1979).
6. K. W. Thompson, *J. Comput. Phys.* **68**, 1 (1987).
7. L. Halpern, *Math. Comput.* **46** (174), 425 (1986).
8. A. Bayliss and E. Turkel, *J. Comput. Phys.* **48**, 182 (1982).
9. A. Bayliss and E. Turkel, *SIAM J. Sci. Statist. Comput.* **3**, 250 (1982).
10. A. Bayliss, M. Gunzburger, and E. Turkel, *SIAM J. Appl. Math.* **42**, 430 (1982).
11. D. H. Rudy and J. C. Strikwerda, *Comput. Fluids* **9**, 327 (1981).
12. F. Nataf, *J. Comput. Phys.* **85**, 104 (1989).
13. G. L. Brown and A. Roshko, *J. Fluid Mech.* **64** (4) 775 (1974).
14. A. Kourta, M. Braza, P. Chassaing, and H. Ha Minh, *AIAA J.* **25** (2), 279 (1987).
15. M. Braza, Thèse de Doctorat d'Etat, Institut National Polytechnique de Toulouse, Toulouse, France, 1986.
16. M. Braza, P. Chassaing, and H. Ha Minh, *Phys. Fluids A* **2** (8), 1461 (1990).
17. M. Braza, P. Chassaing, and H. Ha Minh, *J. Fluid Mech.* **165**, 79 (1986).
18. F. H. Harlow and J. E. Welch, *Phys. Fluids* **8** (12), 819 (1965).
19. M. Braza, H. Ha Minh, and J. B. Cazalbou, "Analyse of Laminair Flow over a Backward Facing Step," Serie: Notes on Numerical Fluid Mechanics, Vol. 9 (Vieweg-Verlag, Brunswick, 1984).
20. B. Freymuth, *J. Fluid Mech.* **25**, 683 (1966).
21. C. M. Ho and P. Huerre, *Ann. Rev. Fluid Mech.* **16**, 365 (1984).
22. G. Jin, Mémoire du D.E.A. (Diplôme d'Etudes Approfondies), Institut National Polytechnique de Toulouse, Toulouse, France, 1989.
23. F. K. Browand and B. O. Latigo, *Phys. Fluids* **22** (6), 1011 (1979).
24. C. M. Ho and L. S. Huang, *J. Fluid Mech.* **119**, 443 (1982).